Tensile and Impact Behavior of Drawn Polystyrene and High-Impact Polystyrene

MITSURU YOKOUCHI, AKITOSHI YOKOTA, and YASUJI KOBAYASHI, *Department of Industrial Chemistry, Faculty of Technology, Tokyo Metropolitan University, Fukazawa, Setagaya-ku, Tokyo 158, Japan*

Synopsis

The tensile behaviors of drawn polystyrene (PS) and high-impact polystyrene (HIPS) were examined systematically in the wide range of strain rate, 1.7×10^{-4}–13.1 m/s, without changing the mode of deformation and the shape of the test pieces. It was found for both PS and HIPS that the flexion points of birefringence with increase of draw ratio are intimately correlated with the tensile properties. Especially, the breaking strain and energy of undrawn and drawn HIPS were assigned to the contributions of the following three toughening mechanisms: (a) the generation of large numbers of microcrazes from the equatorial zone of the dispersed rubber particles; (b) the extension of interfacial rubber phase around the circumpolar zone of the dispersed rubber particles and its disintegration from the matrix component; and (c) the shear band formation of the matrix component followed by cold drawing. These mechanisms were discussed in connection with the factors of stress concentration to the rubber particles, hydrostatic pressure effect arising from the difference in Poisson's ratio of rubber and matrix components, and heat generation due to the adiabatic deformation.

INTRODUCTION

The lack of toughness at service temperature limits the use of plastics in glassy state such as polystyrene (PS) to nonimpact applications. There are a number of ways that this deficiency can, to some extent, be overcome: biaxial orientation, copolymerization, plasticization, increasing molecular weight, use of fillers, and the addition of a rubber material. High-impact polystyrene (HIPS) and poly(acrylonitrile–butadiene–styrene) (ABS) resins have been developed as commercial products by incorporation of fine particles of rubber into matrices of glassy polymers, which makes these materials more resistant to impact breakage than unmodified glassy polymers. The toughening mechanism of the dispersed rubber particle has been extensively investigated. The fractures of HIPS and ABS are usually preceded by an opaque whitening of the stressed area. Bucknall and Smith were the first to associate this stress whitening with microcrazing.[1] This gave rise to the theory of massive crazing, which is based upon the idea that energy is dissipated through the formation of many small crazes rather than in one large crack. This interpretation has been supported by later observations.[2–13] On the other hand, Newman and Strella studied some rubber-modified glassy polymers and argued that the rigid matrix yields and the toughness is a result of the large energy absorption involved in the cold drawing of the matrix, and the rubber phase acts principally to induce a yielding of the matrix.[14–16] Though the interpretation is different from theirs, the similar cold-drawing mechanism has been observed in solution blending of HIPS with polyphenylene oxide (PPO),[17,18] thermoplastic elastomers,[19] and cold-rolled ABS.[20]

Journal of Applied Polymer Science, Vol. 27, 3007–3018 (1982)
 CCC 0021-8995/82/083007-12$02.20

It has been discussed that the improvement in impact resistance of rubber-modified polymer is dependent upon the composition and concentration of rubber, the rubber particle size and morphology, the rubber phase volume (rubber + occluded matrix component), the levels of crosslinking and grafting, and the molecular weight distribution of the matrix polymer.[21–27] Among these factors, we took notice of preorientation of the material, which may change only the effect of rubber particle size and morphology. In fact, the cold-drawing mechanism as well as microcrazing were detected in our drawn HIPS. The present paper is directed to clarify systematically the tensile behaviors of commercial HIPS with various degrees of orientation in the wide range of strain rate (containing impact speed) and to discuss the toughening mechanisms (microcrazing and cold drawing) in detail. When the rubber particle deforms during preextending, the orientation of the matrix component can be expected to occur. Therefore, the similar tensile tests for the preoriented unmodified PS were performed, and the contribution of this to the toughening mechanism was also examined.

EXPERIMENTAL

Specimens

The granules of HIPS (Styron 470, Asahi Dow, T_g = 85°C) were compression-molded (50 kg/cm^2 and 150°C) into sheets of thickness 250 μm, followed by quenching in ice water. A similar procedure was adopted for the granules of PS (Styron 666, Asahi Dow, T_g = 95°C) except for the compression-molded temperature, which was 160°C. In order to obtain samples with different orientation, the molded sheets were placed in an air oven of the uniaxially stretching machine at 105°C for 15 min and drawn to various lengths (up to the maximum draw ratio λ = 7), followed by cooling to room temperature. In the choice of the optimum drawing temperature, the value of birefringence at λ = 5 was used as a measure. Figure 1 shows the relationship between the drawing temperature and birefringences of HIPS and PS. It was found to be desirable to keep the drawing temperature close to T_g (95°C for HIPS and 105°C for PS) to ensure the highest possible molecular orientation, that is, to increase the efficiency of drawing. The present study adopted 105°C as a common drawing temperature for HIPS and PS. Specimens for tensile and impact tensile testings (common shape with substantial dimensions 5 × 58 mm) were prepared from the above elongated sheets.

Density and Birefringence

Densities of the samples were measured at 23°C in a density gradient column composed of water and ethylene glycol. Since PS absorbs water in the gradient column, the position of the specimen was plotted against the root of the measurement time. The observed density was estimated by extrapolation of the curve to zero time.

The degree of birefringence of drawn HIPS and PS was examined through a polarizing microscope with a Berek compensator. The measurements were carried out in Na–D line (589 nm) at room temperature.

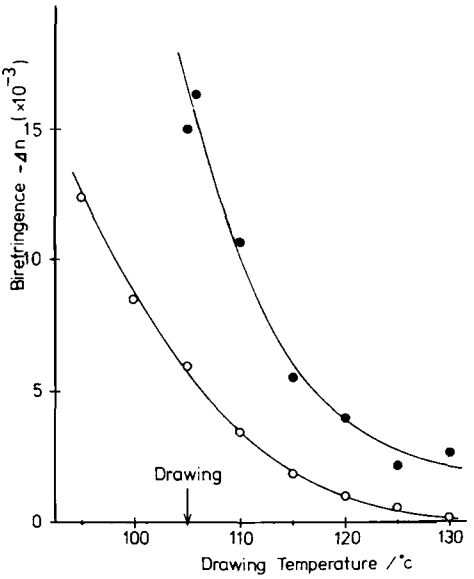

Fig. 1. The relationship betwen the drawing temperature and birefringences of (○) HIPS and (●) PS.

Dynamic Tensile Measurement

In the dynamic tensile measurement, it may be a little difficult to get the exact value of the temperature dispersion properties for the drawn amorphous polymer. Recently, we designed and fabricated a compact apparatus for the study of dynamic mechanical viscoelastic behaviors in polymer solids at any desirable frequency between 10^{-3} Hz and 10^{2} Hz with sufficient driving force.[28] In the present study, only the frequency dispersions of dynamic storage and loss moduli (E' and E'') and loss factor ($\tan\delta$) were measured for the drawn HIPS and PS at the constant temperature (23°C).

Tensile Breaking Tests

Tensile breaking tests were performed over a wide range of strain rates without changing the mode of deformation and the shape of the test pieces. For the lower speed tensile testing, a conventional tensile tester was utilized, which covered the rate of deformation from 1.7×10^{-4} m/s to 2.8×10^{-2} m/s. For the higher speeds, a flywheel-type impact tensile tester was used.[29] The tensile speeds could be easily controlled by changing the revolutions of the flywheel, and in the present study were adopted for the range of 1.3–13.1 m/s. These enabled us to test over 5 decades of strain rate (1.7×10^{-4}–13.1 m/s = 0.29–2.3×10^{4} %/s). The experiments were conducted at 23°C and below a relative humidity of 50%. The numbers of specimens tested per each strain rate were nine for the higher speeds and five for the lower speeds (due to the small scattering of data points in the latter case), and the arithmeric mean and estimated standard deviation were calculated from the set observations. The stress–strain curves gave the following four mechanical quantities: (1) modulus of elasticity E; (2) maximum tensile stress σ_m; (3) extension until failure ϵ_b; and (4) breaking energy indicated by the area under the curve S_b.

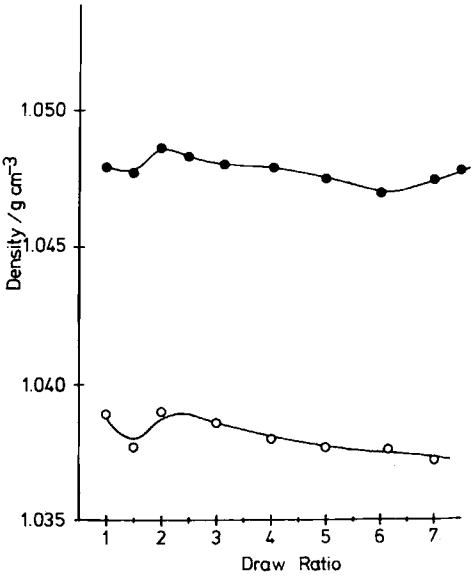

Fig. 2. The change in densities of (○) HIPS and (●) PS with increase of draw ratio.

RESULT AND DISCUSSION

Since no appreciable change of density (Fig. 2) and the external appearance due to the hot drawing at 105°C were observed, microcrazes and/or cracks in both the drawn HIPS and PS specimens were not likely to occur. Figure 3, a transmission micrograph of a section microtomed from a stained specimen of undrawn HIPS, shows the distribution state of the dispersed rubber particles from which PS is occluded. It was, then, considered that the softened PS matrix and rubber particle at 105°C are deformed in the same manner during stretching: The shape of rubber particle would be permanently distorted into a prolated spheroid at room temperature, of which the apse line is aligned in the direction parallel to the drawing one. Such a state of rubber particle in the injection-molded HIPS has been examined by electron microscopy in the etch method.[17] The overall changes in the preorientational behavior of macromolecular chains were evaluated by the measurements of density and birefringence. Figure 4 indicates the

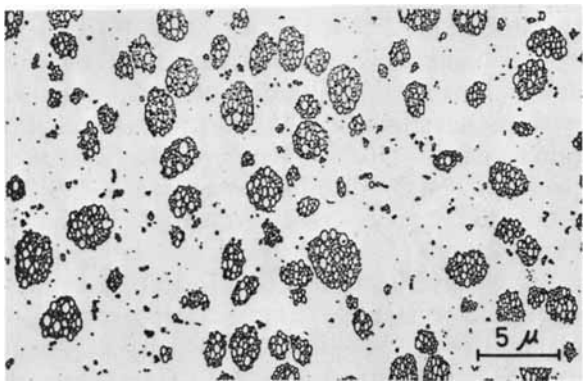

Fig. 3. Transmission micrograph of a section microtomed from a stained specimen of undrawn HIPS.

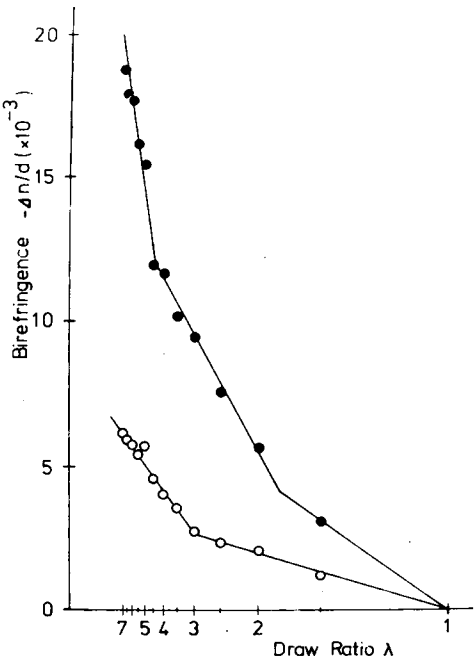

Fig. 4. Variation in birefringences of (○) HIPS and (●) PS with increase of draw ratio.

birefringences of the predrawn HIPS and PS corrected by the observed density ($-\Delta n/d$) plotted against the reciprocal of drawn ratio. Direct comparison of the degree of orientation between HIPS and PS could not be made because the phenyl groups of PS are inclined perpendicular to the drawing direction and this contributes negatively to the average birefringence,[30] while the main chain of PS and polybutadiene do positively. It can be, however, understood from the flexial points in Figure 4 that the substantial changes in the molecular packing manner and orientational behavior occur near to $\lambda = 3$ for HIPS and near to $\lambda = 2$ and 5 for PS, respectively.

We, therefore, expected that such structural changes must be reflected on the tensile mechanical properties. Figure 5 demonstrates the frequency dispersions (from 10^{-2} Hz to 10^{2} Hz) of the dynamic tensile viscoelastic behaviors of some drawn specimens at 23°C. For both HIPS and PS, it was found that, with the increase of draw ratio, $|E|$ increases almost monotonously, $\tan\delta$ decreases slightly, and no appreciable changes of their patterns during the present frequency range occur. This means that in the minute amount of strain region (elastic region) at room temperature, the mechanical properties of HIPS are mainly governed by those of the matrix component, and no features due to the existence of dispersed rubber particles are manifested.

Then, two kinds of tensile breaking tests (at the deformation speeds of 1.7×10^{-4} and 5.3 m/s) were performed for a start in expectation of the strain rate dependency. The changes of maximum tensile stress (σ_m) with an increase of draw ratio are shown in Figure 6, the value of which corresponds to the breaking stress for the case of brittle fracture and to the yield stress for the case of ductile fracture. At low speed, σ_m of PS showed a slightly sharp increase until $\lambda = 2$ and leveled off to about 8×10^{7} Pa. At high speed, σ_m of PS offered the similar

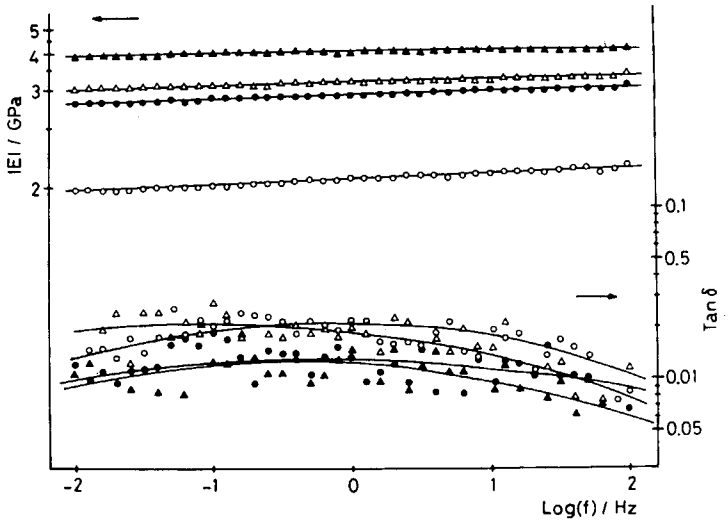

Fig. 5. Frequency dispersion of dynamic mechanical properties of some drawn HIPS (○, ×1.5; ●, ×6) and PS (△, ×1.5; ▲, ×6) at 23°C.

pattern to that in the low speed with large magnitude. HIPS gave almost the similar variation patterns to those of PS with less feature and magnitude. This implies that the tensile strength is also governed by that of matrix component and the dispersed rubber particles only function in decreasing the volume fraction of the hard matrix component. Figure 7 shows the dependence of breaking strain (ϵ_b) on draw ratio for HIPS and PS. The change of ϵ_b in PS increased up to $\lambda = 2$ and indicated the maximum near to $\lambda = 5$. It should be noted that these two draw ratios correspond just to the two flexion points of birefringence in Figure 4. The vague yield phenomenon was observed from $\lambda = 2$, where no shear

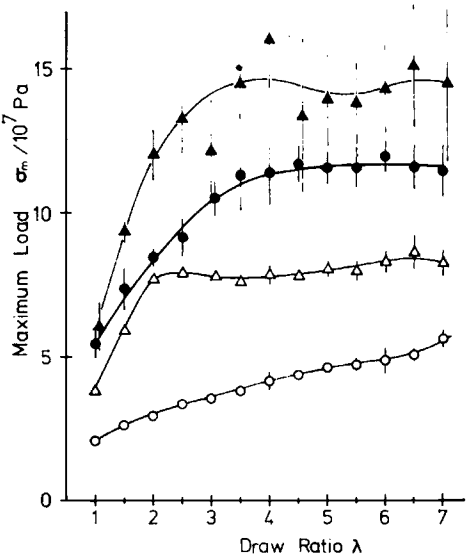

Fig. 6. Dependencies of maximum tensile stress on draw ratio for HIPS and PS. For HIPS: (○) $\dot{\epsilon} = 2.9 \times 10^{-3}$/s; (●) $\dot{\epsilon} = 9.1 \times 10$/s. For PS: (△) $\dot{\epsilon} = 2.9 \times 10^{-3}$/s; (▲) $\dot{\epsilon} = 9.1 \times 10$/s.

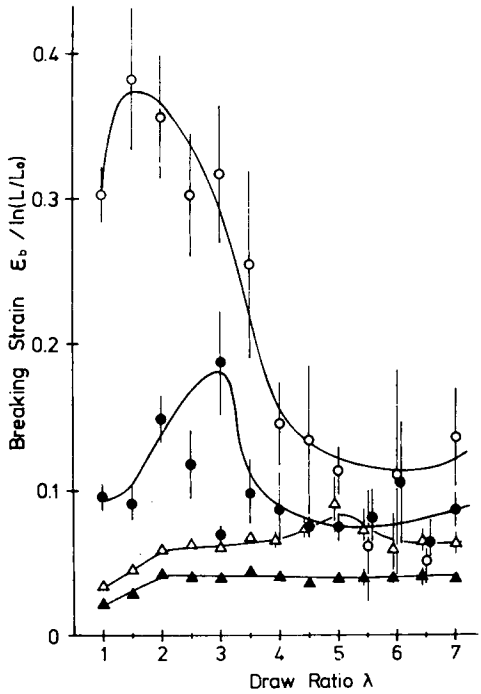

Fig. 7. Dependencies of breaking strain on draw ratio for HIPS and PS. For HIPS: (○) $\dot{\epsilon} = 2.9 \times 10^{-3}$/s; (●) $\dot{\epsilon} = 9.1 \times 10$/s. For PS: (△) $\dot{\epsilon} = 2.9 \times 10^{-3}$/s; (▲) $\dot{\epsilon} = 9.1 \times 10$/s.

yielding or whitening occurred and the fibrous structure[31] became pronounced. Above $\lambda = 5$, cold drawing after clear yield began to be exhibited. A limited number of specimens showed the high elongation to break (60–80%) as reported by other workers,[32,33] but their data were eliminated in Figure 7 because of their poor reproducibility. At any rate, it is clear for PS that there exists an intimate relationship between the change of birefringence and the behavior of breaking strain. On the other hand, the effect of dispersed rubber particles in HIPS became remarkable for the first time in the breaking strain. In the low speed, HIPS offered the maximum of ϵ_b at $\lambda = 1.5$ and leveled off over $\lambda = 4$. The observation of tested specimens indicated that ϵ_b up to $\lambda = 3$ is due to the stress whitening (microcrazing) and the contribution of cold drawing began to appear from $\lambda = 3$. In the high speed, the draw ratio of the maximum shifted to the higher region ($\lambda = 3$) and the cold drawing became a dominant mechanism.

Comparing with PS, HIPS was found to be fairly complicated in the tensile deformation behavior: (1) strong dependencies of ϵ_b on both draw ratio and strain rate and (2) occurrence of two deformation mechanisms (microcrazing and cold drawing). To clarify this complicated phenomenon in HIPS, we tried to examine in detail the strain rate dependent properties for the four kinds of specimens (undrawn and $\lambda = 2$, 3, and 4) in the wide range of deformation speeds (1.7×10^{-4}–13.1 m/s). Figure 8 shows the result of the maximum tensile stress. It was found that the value of σ_m increases roughly semilogarithmically with the tensile speed, and the dependency of it on the draw ratio is also simple. Figure 9 demonstrates the results of the breaking strain. The elongation of undrawn HIPS fell off linearly with the inverse log strain rate in the lower speed region

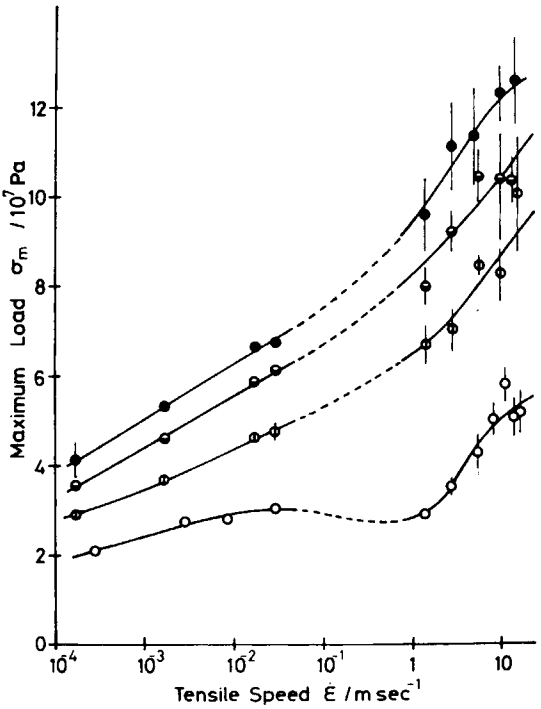

Fig. 8. Strain rate dependencies of maximum tensile stress on draw ratio for HIPS: (○) undrawn; (⊕) ×2; (⊖) ×3; (●) ×4.

and started to level off from 1 m/s, followed by an abrupt increase at 7–10 m/s. The degree of stress whitening just corresponded to the quantity of breaking strain. An interpretation of this behavior was reported in the preceding paper.[34] Its main conclusion was that the characteristic change of ϵ_b in undrawn HIPS originates from the following two main mechanisms (which have different time responses): (A) at low speeds, the generation of large numbers of microcrazes from the equatorial zone of dispersed rubber particles against the tensile direction and (B) at higher speeds, the extension of interfacial rubber around the circumpolar zone of particle and its disintegration from the matrix phase. The mechanism of (B) is promoted in part from a local heat generation due to the adiabatic deformation. The ϵ_b of HIPS at $\lambda = 2$ showed the maximum at about 6.7×10^{-2} m/s and leveled off in the higher speed region, and its magnitude was wholly high compared with undrawn HIPS. Figure 10(a) indicates the external appearance of the broken test pieces of HIPS with $\lambda = 2$ after tensile testings in the various deformation speeds. As can be seen from these photographs, the degree of stress whitening and the quantity of breaking strain were intimately correlated [all specimens of HIPS before testings in the present study were semitransparent as shown in (3)–(6) of Figure 10(b)]. It is noted here that, in the higher speed region, the stress whitening of HIPS with $\lambda = 2$ appears over almost the entire specimen while that of undrawn HIPS was limited to the narrow region at which fracture takes place. This means that the toughening mechanism of (A) at $\lambda = 2$ is dominant and the contribution of (B) to the ϵ_b become less important in its quantity. This phenomenon may be interpreted as follows. The microcrazing mechanism associates with micronecking of the glassy component

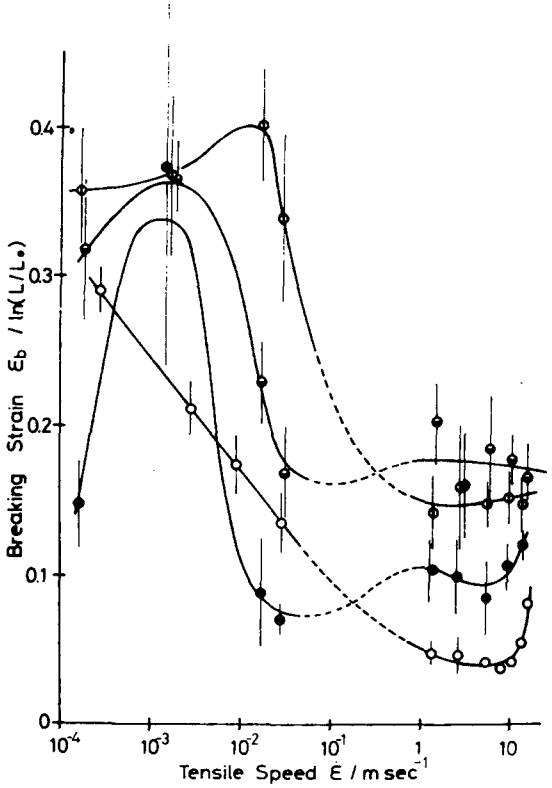

Fig. 9. Strain rate dependencies of breaking strain on draw ratio for HIPS: (○) undrawn; (◔) ×2; (◒) ×3; (●) ×4.

to yield microfibrils, primarily in the equatorial regions of rubber particles.[1–13] The stress concentration level depends on the radius of curvature of the rubber particle at equatorial zone, and there is the optimum size for the generation of the microcrazes at the most efficient rate.[19,21–27] We consider the effect of hot drawing the increase of apparent radius of curvature at the equatorial zone of the dispersed rubber particle without change of rubber volume fraction (deformation from sphere to prolate spheroid). As shown in Figure 3, the present commercial sample is not entirely homogeneous in the rubber particle size distribution, and the small particles are likely to generate excess stress concentrations. In the same quantity of deformation, it is clear that the efficiency of the increase of apparent radius of curvature at the equatorial zone is far higher in the small rubber particle than in the large one. Hot drawing, therefore, apparently makes the rubber particle size distribution at the equatorial zone uniform, which is suited for the thorough generation of microcrazes.

The next subject is how this deformation behavior varies when the draw ratio exceeds $\lambda = 2$, which is assumed optimum for thorough generation of microcrazes. The change of ϵ_b of HIPS with $\lambda = 3$ and 4 are shown in Figure 9. Although these strain rate dependencies seem to resemble the one at $\lambda = 2$, it was found that there exists an essential difference between them. As can be seen from Figure 10(b) (the transparent region around the breakage), the main contribution to ϵ_b at $\lambda = 3$ and 4 was not microcrazing but a new toughening mechanism, i.e., (C) cold drawing. The similar change of tensile deformation mode by sufficient

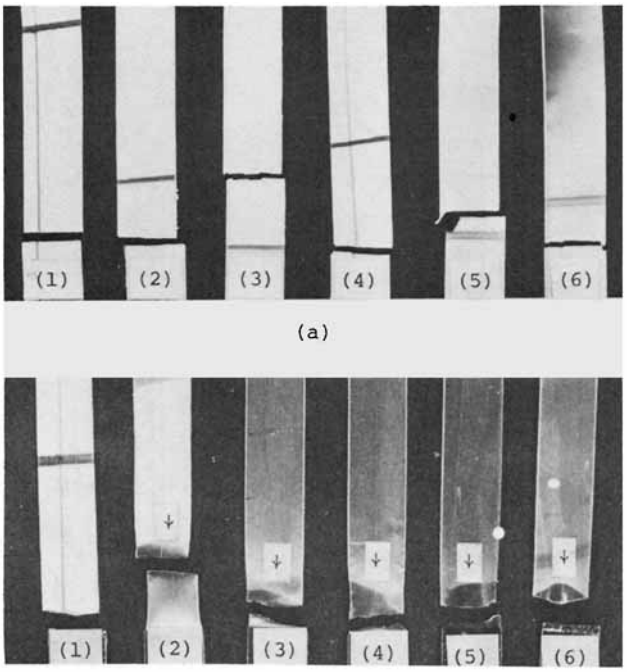

Fig. 10. Photographs of broken test pieces of (a) HIPS, ×2 and (b) HIPS, ×4; deformation speeds (m/s) are: (1) 1.7×10^{-4}, (2) 1.7×10^{-3}; (3) 1.7×10^{-2}; (4) 2.8×10^{-2}; (5) 1.3; (6) 13.1.

rolling have been reported for the case of ABS.[20] Since the draw ratio $\lambda = 3$ just corresponds to the flexion point of birefringence in Figure 4, there must be an intimate relationship between the occurrence of the mechanism of (C) and the substantial changes of orientational behavior in HIPS. This may be interpreted as follows. Certainly, the orientation of the matrix component (PS) near to $\lambda = 3$ is induced to some extent, and this may suppress the occurrence of microcraze which is difficult to propagate in the direction perpendicular to the molecular orientation.[35] This suppression also results from the too large radius of curvature at the equatorial zone of rubber particle to elevate the stress concentration level. During tensile strain, these two factors generate a high hydrostatic pressure state at the boundary of the two phases, which arises from difference in Poisson's ratio (i.e., the matrix tends to increase its volume during strain while the rubber phase tends not to), before the primature microcrazing occurs. There have been two interpretations for the relationship between this hydrostatic pressure effect and the mechanism of cold drawing. (1) Newman and/or Strella proposed a free volume idea: The volume dilation occurring near to the equator of the rubber particle is relatively large, and this results in an increase in the free volume of the matrix to lower the glass transition temperature of the matrix to the point where large-scale molecular motion or cold drawing is favored.[14–16] (2) Kawai and his co-workers, on the other hand, recently emphasized the hydrostatic pressure effect itself upon inducing high plasticity of the glassy matrix component.[19] The latter interpretation was based upon the study of hydrostatic pressure effect on the brittle-to-ductile transition reported by Matsushige et al., where they explained the mechanism of this transition in terms of interaction between competing microplastic deformation processes (crazing and shear

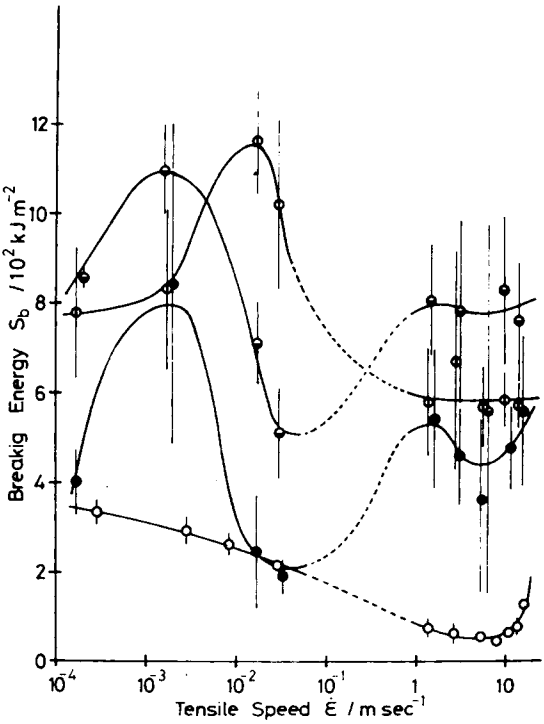

Fig. 11. Strain rate dependencies of breaking energy on draw ratio for HIPS: (○) undrawn; (⊕) ×2; (⊖) ×3; (●) ×4.

banding) which are in quite different pressure dependences, and furthermore refuted the concept of mechanical relaxation phenomena correlated with this transition.[36] As described before, there are two factors for the enhancement of hydrostatic pressure: (α) elevation of resistance for microcraze propagation and (β) prevention of excess stress concentration to the rubber particles. The effect of (α) has been experimentally supported by Bucknall and his co-workers.[18] They clarified in the study of the creep mechanism of HIPS/PPO blends that the shear band formation is dominant and responsible for the increased fracture resistance of matrix component. Since such a shear band formation does not accompany the dilation, we consider at present that the theory of (2) appears to be more appropriate to the initiation of cold drawing of glassy matrix component. In addition to this hydrostatic pressure effect, another effect may be added in the cold drawing mechanism. The careful observation of broken test pieces of HIPS at $\lambda = 4$ [Fig. 10(b)] clarifies the strain rate dependencies of the (A) and (C) mechanisms: (i) the dominancy of (A) at 1.7×10^{-4} m/s, (ii) the coexistence of (A) and (C) at 1.7×10^{-3} m/s, and (iii) the dominancy of (C) over 1.7×10^{-2} m/s. We consider that the advantage of (C) in the higher strain rate region results in part from a local heat generation due to the adiabatic deformation.

Figure 11 shows the toughness (S_b) of drawn HIPS, defined as the total area under the stress–strain curve. The value of S_b may be treated adequately as an approximation of the product of σ_m (Fig. 8) and ϵ_b (Fig. 9). Since the change in the maximum tensile stress was a monotonous increase and the breaking strain

varied in the relatively complicated manner, the pattern of S_b almost resembled the case of ϵ_b. As can be seen from Figure 11, the toughness of HIPS certainly improved by drawing in the whole range of the present deformation speeds. The toughening mechanism of the specimens at $\lambda = 3$ and 4, however, was dominantly the shear band formation followed by cold drawing, and this was inherent in the highly oriented state. Then, as far as molded product of HIPS is concerned, the toughening mechanism of cold drawing may be of no practical use for improvement of toughness. On the other hand, the specimen at $\lambda = 2$ deformed only through the microcrazing mechanism and the quantity of microcrazes (whitening) was far immense, compared with the undrawn material. This suggests that there is room for further improvement in toughness (about five times) of the present HIPS as it holds undrawn, by making the dispersed rubber particles more homogeneous in their size distribution and optimum in their size for thorough generation of microcrazes.

References

1. C. B. Bucknall and R. R. Smith, *Polymer*, **6**, 437 (1965).
2. M. Matsuo, *Polymer*, **7**, 421 (1966).
3. J. A. Schmitt, *J. Appl. Polym. Sci.*, **12**, 533 (1968).
4. M. Matsuo, *Polym. Eng. Sci.*, **9**, 206 (1969).
5. H. Keskkula, *Appl. Polym. Symp.*, **15**, 51 (1970).
6. J. A. Schmitt, *J. Polym. Sci. Part C*, **30**, 437 (1970).
7. R. P. Kambour and R. R. Russel, *Polymer*, **12**, 237 (1971).
8. C. B. Bucknall and D. Clayton, *J. Mater. Sci.*, **7**, 202 (1972).
9. R. P. Kambour, *J. Polym. Sci., Macromol. Rev.*, **7**, 1 (1973).
10. J. A. Mason and R. W. Hertzberg, *J. Polym. Sci., Polym. Phys. Ed.*, **11**, 2483 (1973).
11. P. Beahan, A. Thomas, and M. Bevis, *J. Mater. Sci.*, **11**, 1207 (1976).
12. T. R. Steger and L. E. Nielsen, *J. Polym. Sci., Polym. Phys. Ed.*, **16**, 613 (1978).
13. F. Ramsteiner, *Polymer*, **20**, 839 (1979).
14. S. Newman and S. Strella, *J. Appl. Polym. Sci.*, **9**, 2297 (1965).
15. S. Strella, *J. Polym. Sci. A-2*, **4**, 527 (1966).
16. S. Strella, *Appl. Polym. Symp.*, **7**, 165 (1968).
17. C. B. Bucknall, I. C. Drinkwater, and W. E. Keast, *Polymer*, **13**, 115 (1972).
18. C. B. Bucknall, D. Clayton, and W. E. Keast, *J. Mater. Sci.*, **7**, 1443 (1972).
19. H. Kawai, T. Hashimoto, K. Miyoshi, H. Uno, and M. Fujimura, *J. Macromol. Sci.*, **B17**, 427 (1980).
20. M. R. Grancio, *Polym. Eng. Sci.*, **12**, 213 (1972).
21. G. E. Molau and H. Keskkula, *J. Polym. Sci. A-1*, **4**, 1595 (1966).
22. E. W. Wagner and L. M. Robeson, *Rub. Chem. Tech.*, **43**, 1129 (1970).
23. M. Baer, *J. Appl. Polym. Sci.*, **16**, 1109 (1972).
24. E. P. Chang and A. Takahashi, *Polym. Eng. Sci.*, **18**, 350 (1978).
25. J. Silberberg and C. D. Han, *J. Appl. Polym. Sci.*, **22**, 599 (1978).
26. S. G. Turley and H. Keskkula, *Polymer*, **21**, 466 (1980).
27. E. Sacher, *Polymer*, **21**, 1234 (1980).
28. M. Yokouchi and Y. Kobayashi, *J. Appl. Polym. Sci.*, **26**, 4307 (1981).
29. M. Yokouchi and Y. Kobayashi, *J. Appl. Polym. Sci.*, **24**, 29 (1979).
30. Y. Tanabe and H. Kanetsuna, *J. Appl. Polym. Sci.*, **22**, 1619 (1978).
31. A. E. Zacharides, E. S. Sherman, and R. S. Porter, *J. Appl. Polym. Sci.*, **24**, 3137 (1979).
32. K. J. Cleereman, *Appl. Polym. Symp.*, **24**, 31 (1974).
33. K. Matsumoto, J. F. Fellers, and J. L. White, *J. Appl. Polym. Sci.*, **26**, 85 (1981).
34. M. Yokouchi, H. Uchiyama, and Y. Kobayashi, *J. Appl. Polym. Sci.*, **25**, 1007 (1980).
35. N. R. Farrar and J. Kramer, *Polymer*, **22**, 691 (1981).
36. K. Matsushige, S. V. Radcliffe, and E. Baer, *J. Appl. Polym. Sci.*, **20**, 1853 (1976).

Received October 10, 1981
Accepted March 29, 1982